Understanding the dispersion of coaxial plasmonic structures through a connection with the planar metal-insulator-metal geometry

Peter B. Catrysse[a] and Shanhui Fan
Department of Electrical Engineering and Edward L. Ginzton Laboratory, Stanford University, Stanford, California 94305-4088, USA

(Received 3 March 2009; accepted 13 May 2009; published online 9 June 2009)

We elucidate the dispersion behavior of deep-subwavelength propagating modes in coaxial plasmonic structures by making an explicit connection with the planar metal-insulator-metal geometry. We provide an intuitive picture that allows for a qualitative understanding and a quantitative prediction of the *entire* dispersion behavior, which includes the number of modes at every frequency, the modal propagation constants, the propagation losses, and the cutoff frequencies of propagating modes supported by these technologically important structures. We validate our analytical approach by comparing its predictions to first-principles finite-difference frequency-domain simulations. © *2009 American Institute of Physics*. [DOI: 10.1063/1.3148692]

The optical properties of nanoscale apertures in optically thick metallic films have been intensely researched in the past years due to their fundamental importance in near-field optics and nanophotonics, as well as their practical significance for photonic devices and applications, e.g., filters, near-field probes, optical data storage, and nanolithography.[1,2]

To understand the optical properties of nanoscale apertures, it is crucial to understand their modal dispersion behavior. It is well known that the transmission characteristics of apertures critically depend on whether they allow or prohibit propagating modes.[3,4] Among the different subwavelength apertures that have been analyzed, apertures with a concentric geometry are of particular interest. It was recently shown that arrays of holes with coaxial cross-section can transmit up to 90% of the incident visible light despite subwavelength size and Ohmic losses in the metal.[5] Moreover, these structures are promising candidates for deep-subwavelength low-loss propagation of modes at optical frequencies as well.[6]

In this letter, we point out that the *entire* dispersion behavior of plasmonic structures with a coaxial cross-section (Fig. 1 inset), i.e., formed by a dielectric ring in between a metallic core with radius r_1 and a metallic cladding with radius r_2, can be understood *quantitatively* by starting from a planar metal-insulator-metal (MIM) geometry with thickness $d=r_2-r_1$. In the regime of deep-subwavelength propagating modes where $d \ll r_1, r_2$, we derive an approximate dispersion equation that establishes an explicit connection between a structure with a coaxial cross-section, which has a concentric geometry, and a MIM structure, which has a simpler planar geometry. This approach provides important insights into the behavior of plasmonic coaxial structures. While we discuss the coaxial waveguide structure as an example, the proposed method has much broader applicability and can be extended to provide insights into more complicated concentric waveguide structures as well.

Consider a MIM structure formed using the same metal and dielectric materials as the coaxial structure and with dielectric thickness $d=r_2-r_1$. When d is much smaller than the surface plasmon wavelength, the MIM structure supports a single transverse magnetic mode with its dispersion $(\beta_{\mathrm{MIM}}, \omega)$ described by

$$\tanh\left(k_d \frac{d}{2}\right) = -\frac{k_m \varepsilon_d}{k_d \varepsilon_m}, \tag{1}$$

where $k_m^2=\beta_{\mathrm{MIM}}^2-k_0^2\varepsilon_m$ and $k_d^2=\beta_{\mathrm{MIM}}^2-k_0^2\varepsilon_d$.[7] In this expression, $\varepsilon_{m,d}$ represent the relative permittivities of the metal and the dielectric, and $k_0=\omega/c$ is the free-space wave vector. For the coaxial structure, we assume that the propagating mode has its *total* wave vector determined by the MIM dispersion relation, i.e.,

$$\beta^2 + k_\theta^2 = \beta_{\mathrm{MIM}}^2, \tag{2}$$

where β is the component of the wave vector along the propagation axis (perpendicular to the cross-sectional plane) and k_θ is the transverse component in the cross-sectional plane (there is no component in the radial direction). Further observing that structures with cylindrical geometry close on themselves, and hence

$$k_\theta 2\pi r = 2\pi\nu, \tag{3}$$

where ν is an integer. Combining Eqs. (1)–(3), we obtain the dispersion relation for the coaxial structure, which relates the propagation constant β of each mode to its angular frequency ω,

$$\tanh\left(\sqrt{\beta^2+(\nu/r)^2-k_0^2\varepsilon_d}\,\frac{d}{2}\right) = -\frac{\varepsilon_d\sqrt{\beta^2+(\nu/r)^2-k_0^2\varepsilon_m}}{\varepsilon_m\sqrt{\beta^2+(\nu/r)^2-k_0^2\varepsilon_d}}. \tag{4}$$

In this expression, $r=(r_1+r_2)/2$ and ν is an integer representing angular momentum. Equation (4) establishes an explicit connection between the dispersion behavior of the coaxial structure and the planar MIM structure. It allows us to estimate *all features* of the dispersion behavior of deep-subwavelength modes supported by a coaxial structure for which $d \ll r_1, r_2$. We note that related to our effort here, there has been recent work in establishing a relationship between the dispersion of plasmonic modes propagating on a nanowire geometry and those propagating on a single planar interface.[8]

[a]Electronic mail: pcatryss@stanford.edu.

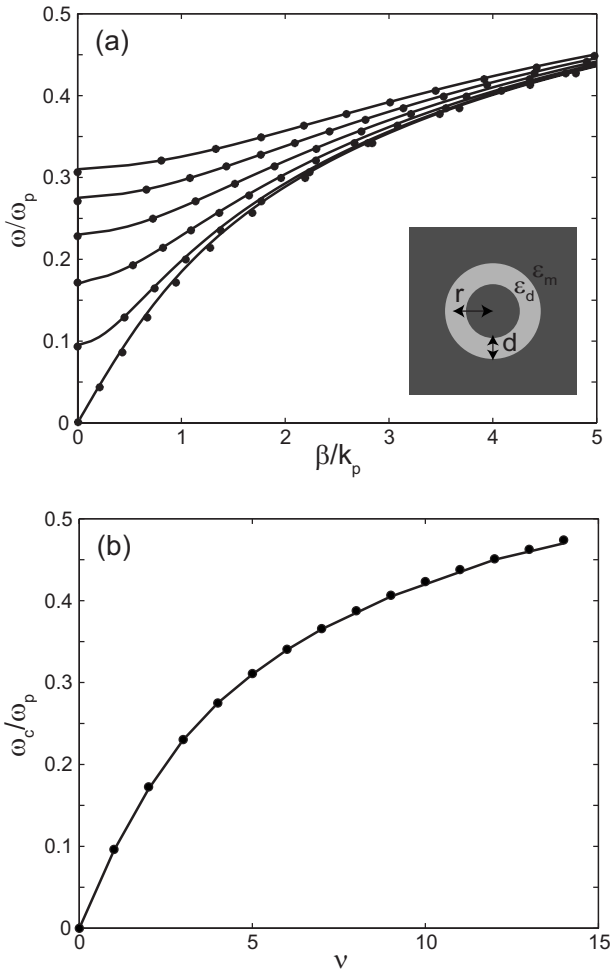

FIG. 1. Propagating modes supported by a structure with coaxial cross-section for a plasmonic metal without loss. (a) Dispersion diagram (β,ω), where β is the real propagation vector along the longitudinal axis of the waveguide and ω is the radial frequency. (b) Cutoff frequency of the modes vs angular momentum ν. The curves are obtained from the analytical expression (solid lines) and from a numerical FDFD method (filled circles). Inset shows the geometry and identifies the average radius $(r=0.345\lambda_p)$ and the width $(d=0.036\lambda_p)$ of the dielectric ring, where λ_p is the plasma wavelength of the metal.

We now verify the results of Eq. (4) against a direct solution of dispersion relation (β,ω) of a coaxial structure using an exact one-dimensional finite-difference frequency-domain (FDFD) method in cylindrical coordinates (r,θ,z).[9] We solve the dispersion equation first, when the material properties of metals at optical frequencies are described by a lossless plasmonic model with plasma frequency ω_p,

$$\varepsilon_m(\omega) = 1 - \frac{\omega_p^2}{\omega^2}. \tag{5}$$

Such a plasmonic model has been the source of valuable insights since it provides a description of the general behavior of real metals in the optical frequency range. Without loss of generality, we fix the relative permittivity of the dielectric material of the waveguides to be $\varepsilon_d=2.13$.

Figure 1 shows the dispersion diagram (panel a) and the cutoff frequency (panel b) of the propagating modes that are supported by a waveguide structure with coaxial cross-section for the case of a lossless plasmonic metal. The first six modes with angular momentum $\nu=0,\ldots,5$ are graphed for a coaxial waveguide with average radius $r=0.345\lambda_p$ and

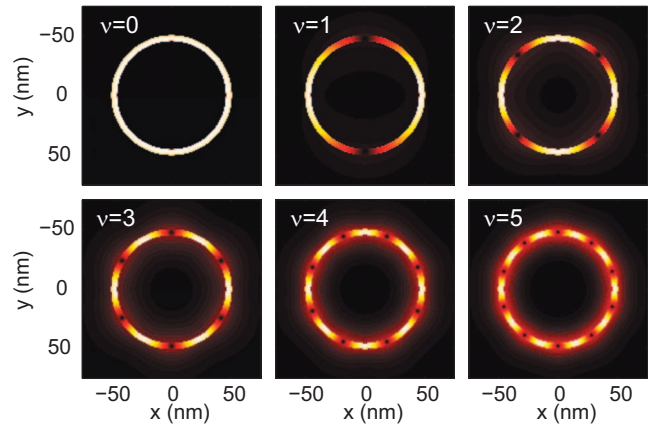

FIG. 2. (Color) Electric field amplitudes of the first six lowest-order modes $(\nu=0,\ldots,5)$ supported by a coaxial structure at their cutoff frequencies $(\omega_{c0}\cong 0,\ \omega_{c1}=0.096\omega_p,\ \omega_{c2}=0.173\omega_p,\ \omega_{c3}=0.230\omega_p,\ \omega_{c4}=0.275\omega_p,$ and $\omega_{c5}=0.311\omega_p)$. The parameter values for the coaxial structure and the material model are the same as those in Fig. 1.

dielectric width $d=0.036\lambda_p$. The analytical theory of Eq. (4) (solid lines) and the numerical FDFD results (closed circles) show excellent agreement.

The use of the analytical theory of Eq. (4) provides important insights about the modes of the structure. One important consequence of Eq. (4) is that the fundamental $(\nu=0)$ mode of a coaxial waveguide has *identical* dispersion to that of a MIM structure. In both cases, the fundamental mode has no cutoff frequency $(\omega_{c0}=0)$, covers the spectral range from dc to surface plasmon frequency $(\omega_{sp}=\omega_p/\sqrt{1+\varepsilon_d})$, and is located entirely below the light line. This explicit quantitative agreement has not been pointed out before.

The theory also indicates the existence of higher-order modes [Fig. 1(a)] and provides a quantitative prediction of their dispersion curves including cutoff [Fig. 1(b)]. For modes with angular momentum $\nu>0$, there always exists a cutoff frequency below which such modes become evanescent and no longer propagate. For this structure, the analytical theory predicts the cutoff frequencies for the first five higher-order modes $(\nu=1,\ldots,5)$ as $\tilde{\omega}_{c1}=0.097\omega_p$, $\tilde{\omega}_{c2}=0.175\omega_p$, $\tilde{\omega}_{c3}=0.233\omega_p$, $\tilde{\omega}_{c4}=0.276\omega_p$, and $\tilde{\omega}_{c5}=0.312\omega_p$. These values are in excellent agreement with the cutoff frequencies $\omega_{c1}=0.096\omega_p$, $\omega_{c2}=0.173\omega_p$, $\omega_{c3}=0.230\omega_p$, $\omega_{c4}=0.275\omega_p$, and $\omega_{c5}=0.311\omega_p$ obtained from numerical FDFD calculations (<1% difference). Above the cutoff frequency, higher-order modes exhibit discrete spectral bands that end at the surface plasmon frequency for asymptotically large values of the propagation constant β [Fig. 1(a)]. The cutoff frequency of these modes also grows with angular momentum and approaches the surface plasmon frequency for very large ν [Fig. 1(b)]. The spectral bands, therefore, become increasingly flat and group velocity $(\partial\omega/\partial\beta)$ decreases, leading to "slow" modes.

Figure 2 shows the electric fields for the fundamental mode near dc $(\omega\cong 0)$ and for five higher-order modes $(\nu=1,\ldots,5)$ at cutoff $(\omega=\omega_{c\nu})$. The field patterns display increasing numbers of nodes corresponding to the angular momentum of the mode. While the fundamental mode with zero angular momentum $(\nu=0)$ does not have a cutoff frequency, it does not couple to incident planes waves due to a mismatch in field symmetry. The next-higher-order $(\nu=1)$ mode with a cutoff, on the other hand, does exhibit proper

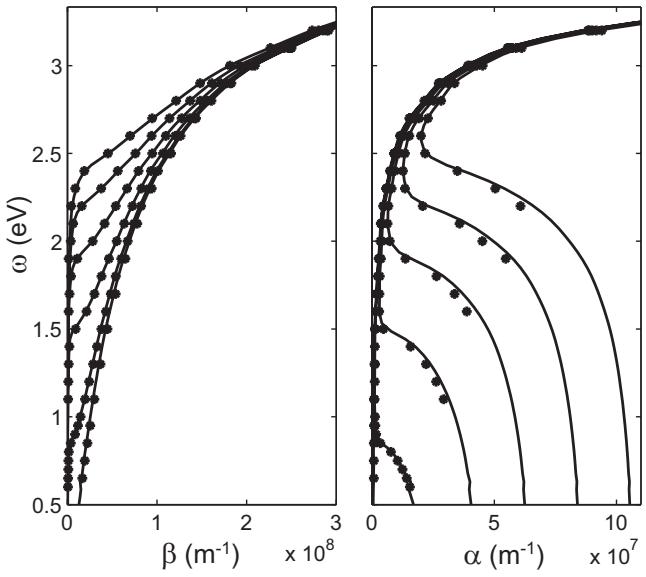

FIG. 3. Dispersion diagram (β,ω) and (α,ω) of the lowest-order modes supported by a coaxial structure for tabulated properties of silver that include material losses. β and α are the real and imaginary parts of the complex propagation vector along the longitudinal axis of the waveguide, and ω is the radial frequency. The curves are obtained from the analytical expression (black lines) and from a numerical FDFD method (filled circles). The average radius $r=47.5$ nm and the width $d=5$ nm.

dipole symmetry and provides an efficient channel for light transport. Since the effective index of the MIM mode goes up as the thickness of the dielectric decreases, the cutoff frequency of this mode also decreases as the thickness is reduced, even when the average radius of the coaxial structure is kept the same. This behavior was observed, but not explained, and it is distinctively different from that of the perfectly conducting coaxial waveguide.[6]

We note that Eq. (4) is not restricted to the plasmonic free-electron model, but rather is valid for measured metal properties as well. Figure 3 shows the dispersion diagram for a coaxial waveguide structure made of silver and dielectric $(\varepsilon_d=2.13)$ with an average radius of 47.5 nm and a dielectric ring width of 5 nm. We used tabulated values for the complex dielectric constant of silver when solving the analytical dispersion [Eq. (4)].[10] We plot the real (β) and imaginary (α) parts of the complex propagation constant $\beta+i\alpha$ as a function of frequency ω in panels (a) and (b). We find that the agreement between the analytical and numerical calculations is excellent for both the real and imaginary parts of the propagation constant. This confirms the validity of the analytical expression in the most general case of tabulated material data that include Ohmic material losses.

As seen from Fig. 3(b), the mode with the lowest loss is the fundamental mode $(\nu=0)$, which has no cutoff. In the presence loss, the definition of cutoff for higher-order modes $(\nu>0)$ is no longer exact.[11] As the frequency is increased, each of these modes goes through a transition from being primarily evanescent (i.e., $|\alpha|\gg|\beta|$) to primarily propagating, (i.e., $|\alpha|\ll|\beta|$). The frequency at which such transition occurs can be used as a practical definition of cutoff. In general, the agreement between the theory of Eq. (4) and numerical simulation is excellent in the frequency range above, near and just below the cutoff frequency. At frequencies much below cutoff, the modes are highly evanescent, and it becomes numerically difficult to isolate the modes of interest from all the other complex modes of the systems. The higher-order modes exhibit increasingly higher propagation losses, although this becomes only significant at frequencies far above the cutoff frequency. At or near the cutoff frequency, the higher order modes have propagation losses that are comparable to that of the low-loss fundamental mode.

As a final note, we comment on the regime of validity for the approximation involved in our approach. The dispersion equation Eq. (4) is a good approximation for $d\ll r_1,r_2$. When d is an order of magnitude smaller than r_1,r_2, for example, the difference in dispersion diagrams between the approximate dispersion equation and the exact results is only a few percent. This regime of validity is also the regime of most interest, i.e., the regime where these structures support deep-subwavelength propagating modes. Moreover, good agreement for the fundamental $(\nu=0)$ mode requires that the metallic core radius r_1 is not too small, to prevent the fields from going to zero due to penetration in the metal. For higher-order $(\nu>0)$ modes this is not a requirement, as the fields in cylindrical geometry go to zero as r_1 goes to zero, and the agreement remains very good even for very small metallic cores.

In summary, we elucidated the dispersion behavior of deep-subwavelength propagating modes in coaxial plasmonic structures by making an explicit connection with the planar MIM geometry. Our approach provides an intuitive picture of the dispersion behavior of deep-subwavelength modes in these technologically important structures. Moreover, it also has broader applicability and can be easily extended to provide insights into more complicated concentric structures as well.

This work was supported by the Stanford Global Climate and Energy Project, the NSF-NIRT Program (Contract No. ECS-0507301), the DOE (Contract No. DE-FG 07ER46426). The computation was performed with support from the NSF-LRAC program.

[1]For an overview, see the focus issue on "Extraordinary light transmission through sub-wavelength structured surfaces," Opt. Express **12** (2004).
[2]T. W. Ebbesen, H. J. Lezec, H. F. Ghaemi, T. Thio, and P. A. Wolff, Nature (London) **391**, 667 (1998).
[3]F. I. Baida and D. Van Labeke, Phys. Rev. B **67**, 155314 (2003).
[4]J. A. Porto, F. J. Garcia-Vidal, and J. B. Pendry, Phys. Rev. Lett. **83**, 2845 (1999).
[5]Y. Poujet, J. Salvi, and F. I. Baida, Opt. Lett. **32**, 2942 (2007).
[6]F. I. Baida, A. Belkhir, D. Van Labeke, and O. Lamrous, Phys. Rev. B **74**, 205419 (2006).
[7]H. Raether, *Surface Plasmons on Smooth and Rough Surfaces and on Gratings* (Springer, Berlin, 1988).
[8]M. A. Schmidt and P. S. J. Russell, Opt. Express **16**, 13617 (2008).
[9]F. Wu, S. P. Guo, K. Ikram, S. Albin, H. Tai, and R. S. Rogowski, Opt. Commun. **249**, 165 (2005).
[10]E. D. Palik and G. Ghosh, *Handbook of Optical Constants of Solids* (Academic, Orlando, 1985).
[11]L. Novotny and C. Hafner, Phys. Rev. E **50**, 4094 (1994).